

# Hydrogen-doping stabilized metallic VO<sub>2</sub> (R) thin films and their application to suppress Fabry-Perot resonances in the terahertz regime

Yong Zhao,<sup>1</sup> Gulten Karaoglan-Bebek,<sup>2</sup> Xuan Pan,<sup>1</sup> Mark Holtz,<sup>3</sup> Ayrton A. Bernussi,<sup>1</sup> and Zhaoyang Fan<sup>1,a)</sup>

<sup>1</sup>Department of Electrical and Computer Engineering and Nano Tech Center, Lubbock, Texas 79409, USA

<sup>2</sup>Department of Physics and Nano Tech Center, Lubbock, Texas 79409, USA

<sup>3</sup>Department of Physics and MSEC, Texas State University, San Marcos, Texas 78666, USA

(Received 23 April 2014; accepted 6 June 2014; published online 16 June 2014)

We demonstrate that catalyst-assisted hydrogen spillover doping of VO<sub>2</sub> thin films significantly alters the metal-insulator transition characteristics and stabilizes the metallic rutile phase at room temperature. With hydrogen inserted into the VO<sub>2</sub> lattice, high resolution X-ray diffraction reveals expansion of the V-V chain separation when compared to the VO<sub>2</sub>(R) phase. The donated free electrons, possibly from O-H bond formation, stabilize the VO<sub>2</sub>(R) to low temperatures. By controlling the amount of dopants to obtain mixed insulating and metallic phases, VO<sub>2</sub> resistivity can be continuously tuned until a critical condition is achieved that suppresses Fabry-Perot resonances. Our results demonstrate that hydrogen spillover is an effective technique to tune the electrical and optical properties of VO<sub>2</sub> thin films. © 2014 AIP Publishing LLC. [<http://dx.doi.org/10.1063/1.4884077>]

VO<sub>2</sub> exhibits a metal-insulator transition (MIT) at a critical temperature  $\sim 68^\circ\text{C}$ , which is accompanied by a crystal structure transformation from the metallic rutile (R) phase to the insulating monoclinic (M1) phase. It has been intensively studied to understand the fundamental mechanisms that govern its phase transition<sup>1-3</sup> and to develop applications including electrical and optical switches.<sup>4,5</sup> The 3–5 orders of magnitude change in electrical conductivity across the MIT are accompanied by a dramatic variation in its dielectric function. In the terahertz (THz) frequency range, the transparent insulating state becomes almost opaque upon crossing the MIT. Therefore, employing the tunable optical properties of VO<sub>2</sub> for THz wave modulation and filtering<sup>6-8</sup> has attracted significant attention when considering that very few natural materials have properties suitable for THz wave manipulation.

Recently, it was demonstrated that VO<sub>2</sub> thin films can be used to suppress Fabry-Perot reflections by tuning its electrical resistivity with temperature during the MIT,<sup>9</sup> a critical need for THz spectroscopy and imaging applications. As shown in Fig. 1(a), when a single THz pulse traverses an optical component, additional transmitted pulses can be observed (Fig. 1(b)) as a result of multiple reflections at its surfaces. This Fabry-Perot resonance effect leads to undesirable frequency and incidence-angle dependence which may considerably impair the performance of THz of systems. Therefore, suppression of this resonance is in great needs. Traditional anti-reflection methods (AR), such as quarter-wave AR coatings,<sup>10</sup> for operation at THz frequencies, would require multiple layers with total thickness as large as several millimeters. These stacks enhance transmission when a beam propagates from a low to high-index medium, but it cannot eliminate the multiple reflections shown in Fig. 1(a). Recently, nanometer-thick metallic films<sup>11,12</sup> were reported as coating materials to eliminate this resonance, as illustrated in Fig. 1(c). This was realized by controlling the film conductance, via thickness variation, until the desired impedance

matching condition (IMC) was achieved. In principle, any thin film whose electrical conductivity matches the critical conductivity has the potential to eliminate the Fabry-Perot resonances. This can be understood from Fig. 1(d). The THz signal is incident from the substrate, with an impedance of  $Z_S$ , to the air with an impedance of  $Z_{air}$ . The conducting film acts as shunt impedance ( $Z_F$ ), in parallel with  $Z_{air}$ . To eliminate the reflection at the substrate/air interface, the load impedance ( $Z_{air}/Z_F$ ) must match with  $Z_S$ , or

$$Z_0 \sigma d = n_S - n_{air}, \quad (1)$$

where  $Z_0$  is the impedance of free space,  $\sigma$  and  $d$  are the critical conductivity and thickness of the film, respectively, and  $n_S$  and  $n_{air}$  are the refractive index of the substrate and air, respectively. Our previous study demonstrated that VO<sub>2</sub> films can be used to suppress Fabry-Perot resonances.<sup>9</sup> However, this involves precise control of the sample temperature during the MIT to achieve the required IMC, which may be difficult to obtain in many applications. Therefore, exploring other approaches, which eliminate the need of temperature control, is of critical importance.

In addition to thermally induced phase transition, the electrical and optical properties of VO<sub>2</sub> thin films may also be tuned using alternative methods. These include vacancy based native-defect doping<sup>13</sup> by control of material growth temperature<sup>14,15</sup> and oxygen flow rate,<sup>16</sup> and through substitutional chemical doping. There has been a continuing interest in controlling the phase transition temperature of VO<sub>2</sub> by chemical substitution.<sup>17</sup> Doping by higher valence elements, such as W, Mo, and Nb, was shown to appreciably reduce the transition temperature.<sup>17,18</sup> These electron donors weaken the V-V pair,<sup>19</sup> and the lattice expansion breaks the Peierls-paired V ions,<sup>20</sup> promoting a reduction of the transition temperature.<sup>21</sup> Moreover, incorporation of the electron donor hydrogen was also reported to be effective in reducing the transition temperature of VO<sub>2</sub>.<sup>22</sup> So-called hydrogen spillover from catalytic metal sites into the supporting oxide

<sup>a)</sup>Zhaoyang.Fan@ttu.edu

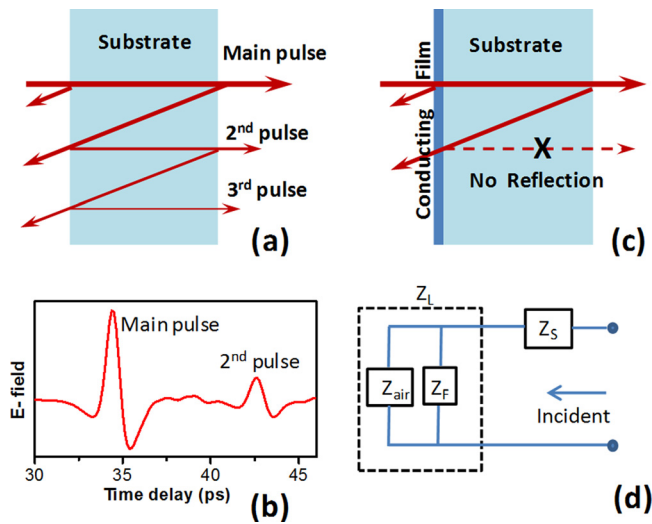


FIG. 1. (a) Schematic of multiple reflections at the air-substrate interfaces. (b) Representative THz transmission of a sapphire substrate. (c) Schematic illustration indicating the suppression of the multiple reflections when the resistivity of VO<sub>2</sub> is tuned to IMC. (d) Schematic of impedance matching circuit for incident signal from the substrate to air.

at low temperatures (<200 °C) has been demonstrated as an effective method for hydrogen doping in several oxides.<sup>23,24</sup> The metal surface provides catalytic sites for breaking the H-H bond and consequent migration of the atomic H into the underlying oxide material.<sup>23</sup> This technique has been used for hydrogen-doped VO<sub>2</sub> powder<sup>25</sup> and nano-beams<sup>26</sup> and was proven to be an effective method to alter the electrical resistivity and MIT characteristics of VO<sub>2</sub>. As a post-growth doping process, hydrogen spillover offers flexibility for resistive control of VO<sub>2</sub> thin films at room temperature (RT).

Here, we apply the hydrogen spillover approach for doping control of VO<sub>2</sub> to tune its RT electrical conductivity. We find that hydrogen doping permits the formation of stable R-phase VO<sub>2</sub> at RT and demonstrate a viable approach to suppress Fabry-Perot reflections.

VO<sub>2</sub> thin films with thickness of ~120 nm were grown on c-plane (0001) sapphire substrates by reactive DC magnetron sputtering. The details can be found in Ref. 27. Nominally, 2 nm thickness of Au was deposited on the VO<sub>2</sub> layer to form sparsely distributed nanoparticle islands which will serve as the H<sub>2</sub> catalyst. The coated VO<sub>2</sub> samples were loaded into a vacuum tube furnace for hydrogen processing. The samples were exposed to H<sub>2</sub> ambient for 20 min with a flow rate of 100 SCCM and a pressure of 50 Torr. We experimented with furnace temperatures ranging from 100 to 200 °C to determine the optimum temperature to achieve the VO<sub>2</sub> resistivity corresponding to the IMC at THz frequencies. Van der Pauw method was used to measure temperature-dependent resistivity curves. High-resolution X-ray diffraction (XRD) was carried out to study structural changes resulting from hydrogen processing and backed by Raman spectroscopy. Normal-incidence terahertz time-domain spectroscopy (THz-TDS) transmission was used to validate the performance of VO<sub>2</sub> film. Two photoconductive antennas were used for THz generation and detection. A mode-locked fiber laser centered at ~1560 nm wavelength with 90 fs pulse duration and 100 MHz repetition rate were split into equal intensity beams (~35 mW) and then focused independently on the surface of

each photoconductive antenna. The bandwidth of the THz system (in air without any sample) is limited to ~2.0 THz. THz transmission experiments and XRD measurements on non-hydrogenated Au-coated VO<sub>2</sub> films revealed similar phase transition characteristics to those observed for uncoated and undoped VO<sub>2</sub> films.

The RT resistivity of the VO<sub>2</sub> films starts to change upon hydrogen processing above 100 °C. Below this temperature, the rate of H<sub>2</sub> decomposing into H on Au catalyst and diffusion into the VO<sub>2</sub> is kinetically limited. The VO<sub>2</sub> resistivity decreases with hydrogen processing temperatures to 160 °C, above which no obvious further drop in resistivity was observed. We focus on three samples. S1 is the as-grown VO<sub>2</sub> thin film that did not experience hydrogen processing. Gold-coated S2 and S3 were processed in hydrogen at temperatures 135 and 160 °C, respectively.

The temperature dependent resistivity is plotted in Fig. 2. The resistivity curve of S1 indicates that the as-grown sample is in the insulating state with a resistivity of ~20.0 Ω cm at RT and transforms into its metallic R-phase at temperatures beyond 356 K with a resistivity of ~4 × 10<sup>-4</sup> Ω cm. The resistivity dramatically differs upon hydrogen doping at 135 °C. At RT, S2 exhibits a value of 2.50 × 10<sup>-3</sup> Ω cm, a reduction of nearly four orders of magnitude when compared with the as-deposited material. At high temperatures, the resistivity of S2 is comparable to that of S1, consistent with transformation into the metallic state. Therefore, the 135 °C hydrogen processing suppresses the resistivity change across the MIT to less than one order of magnitude. We also observe that the phase transition temperatures are significantly lower, and the hysteresis window is greater than the unprocessed VO<sub>2</sub>. When the hydrogen processing temperature was increased to 160 °C, S3 sample has low resistivity at RT. This value is close to those measured for VO<sub>2</sub> films in the metallic state. Therefore, no obvious MIT is observed in Fig. 2 for S3 in the temperature range of our measurement. In this temperature range, S3 is in the metallic rutile phase, as will be explained later.

The results shown in Fig. 2 confirm that hydrogen incorporation modifies the electrical properties of the VO<sub>2</sub>. However, as discussed in Ref. 15, V<sup>3+</sup> related phases can also introduce a similar resistivity change in VO<sub>2</sub> thin films, considering that in the present study hydrogen may reduce V<sup>4+</sup> to V<sup>3+</sup>. Corundum V<sub>2</sub>O<sub>3</sub> itself is a metallic conductor at RT with a resistivity close to the metallic VO<sub>2</sub> (R).<sup>28</sup> In the

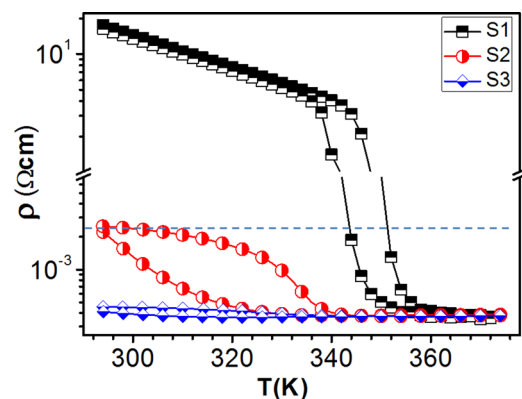


FIG. 2. Temperature dependent resistivity curves for S1-S3. The dashed straight line corresponds the expected IMC resistivity for VO<sub>2</sub>/sapphire.

current context, this seems implausible since it would correspond to substantial changes in the stoichiometry due to the hydrogen processing. To investigate off-stoichiometry phase formation upon H<sub>2</sub> processing, we performed XRD measurements in all three samples.

Fig. 3(a) displays the RT  $\theta$ - $2\theta$  XRD data. The Al<sub>2</sub>O<sub>3</sub> (0006) peak at 41.73° serves as reference for accurate angle determination. The peak at P1 = 39.88° for S1 is from VO<sub>2</sub> (020)<sub>M1</sub> diffraction,<sup>6</sup> unambiguously identifying it as the expected monoclinic phase (in what follows, subscripts M1 and R represents M1 and R structures, respectively). S3 exhibits a distinctive peak denoted as P2 at smaller  $2\theta$  angle of 39.45°. The S2 XRD pattern consists of two sub-peaks close to P1 and P2. The two-peak diffraction pattern suggests a mixture of two structural phases in S2, but no evidence of additional phases is obtained.

Based on JCPDS standard,<sup>29</sup> the 39.45° P<sub>2</sub> peak from S3 in Fig. 3(a) cannot be assigned to any diffraction peak of V<sub>2</sub>O<sub>3</sub>, thereby ruling it out as a plausible interpretation for the low-resistivity material in this sample. The low resistivity of S3 is due to hydrogen-doping stabilized RT VO<sub>2</sub>(R) phase, and the P2 peak is the (200)<sub>R</sub>-plane diffraction from tetragonal R-phase VO<sub>2</sub>. This is because the monoclinic (020)<sub>M1</sub> plane in VO<sub>2</sub> transforms to the (200)<sub>R</sub> plane upon MIT. This interpretation was further confirmed by performing XRD scans at different sample temperatures. Figure 3(b) shows XRD patterns of sample S1 at RT and at 368 K, corresponding to the M1-phase and the R-phase, respectively. A distinctive peak shift was observed from 39.88° (020)<sub>M1</sub> peak at RT to 39.67° (200)<sub>R</sub> peak at high temperature. A similar shift in temperature-dependent XRD was reported across the MIT of VO<sub>2</sub> thin films with a gradual transition at intermediate temperatures.<sup>30</sup> The reduction in  $2\theta$  value is caused by the expansion of V-V chain length due to unpairing of the tilted V-V zigzag chain in the monoclinic structure to form linear V-V chains during structural transition into R phase.<sup>31</sup> However, the P2 diffraction angle of S3 deviates

from the standard VO<sub>2</sub> (200)<sub>R</sub> value by  $\sim -0.2^\circ$ . The smaller P2 angle suggests further V-V chain expansion caused by atomic hydrogen doping. Based on Bragg's law, a plane spacing of 2.26 Å was calculated for P1 (M1 phase), 2.27 Å for VO<sub>2</sub> (200)<sub>R</sub> peak (R phase), and a further expanded plane spacing of 2.28 Å for P2 (hydrogenated VO<sub>2</sub>(R) phase). The lattice expansion of hydrogenated VO<sub>2</sub> from undoped VO<sub>2</sub> rutile structure suggests that hydrogen inserts into VO<sub>2</sub> resulting in lattice distortion.

Molecular hydrogen dissociates on catalytic Au surface into atomic hydrogen, diffuses, and intercalates into the underlying VO<sub>2</sub> film. Because of its low electronegativity, H bonds with the high-affinity oxygen atom of the V-O-V chain to form strong H-O bond and maintains V-OH-V structure.<sup>25,26</sup> This is similar to the bond formation of hydrogen dopants in rutile TiO<sub>2</sub>.<sup>24</sup> Since hydrogen will contribute one electron when forming the OH<sup>-</sup> group, the donated electrons lead to stronger electron-electron correlation in VO<sub>2</sub> and hence stabilize the metallic rutile structure to temperatures lower than  $\sim 68^\circ\text{C}$ , the transition temperature of undoped VO<sub>2</sub>.<sup>22,26</sup> In addition, the expansion of lattice plane after hydrogenation, as indicated by XRD measurement, reduces overlap of electron waves of neighboring vanadium atoms, and therefore further suppressing the tendency of Peierls dimerization. This explains the low resistivity of hydrogenated S2 and S3 and the reduced transition temperatures. The XRD data for S2 support a superposition of M1 and R phases of VO<sub>2</sub>. Therefore, the low hydrogen processing temperature does not fully hydrogenate the sample to produce homogeneous VO<sub>2</sub>(R); instead, coexisting VO<sub>2</sub>(M1) and VO<sub>2</sub>(R) phases are present. The integrated RT intensity of P2 over P1 for S2 gives a rough estimation of the volume fractions  $\sim 56\%$  and  $44\%$ , respectively, of these two phases in S2.

Figure 4 shows the Raman spectra of S1-S3 measured at RT under identical excitation/detection conditions. The Raman peaks verify the presence of M1-phase in S1 and S2.<sup>32</sup> Since the R phase is metallic, it exhibits negligible Raman intensity. Thus, the lower Raman intensity in sample S2 is consistent with the mixture of M1 and R phases determined from the XRD experiments. The absence of Raman peaks from S3 is consistent with the interpretation that this sample is at the metallic rutile phase at RT. Most importantly, we observe no evidence of alternative vanadium oxide phases in S2. This is consistent with our conclusion,

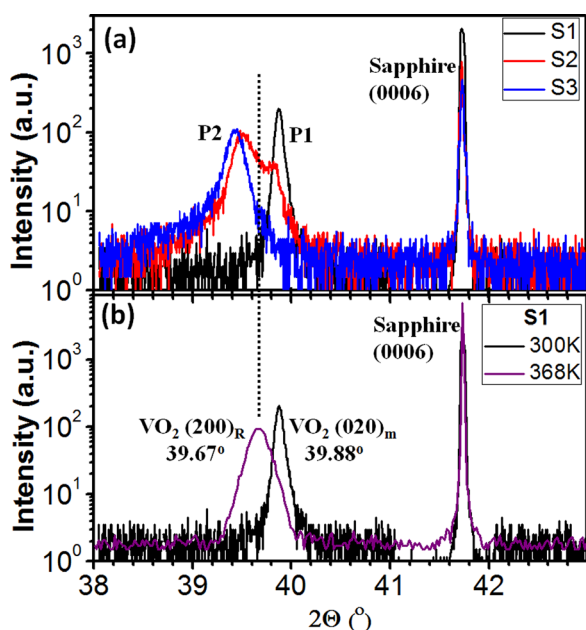


FIG. 3. XRD  $\theta$ - $2\theta$  scan patterns of S1-S3 in (a) and S1 at 300 K and 368 K temperatures in (b).

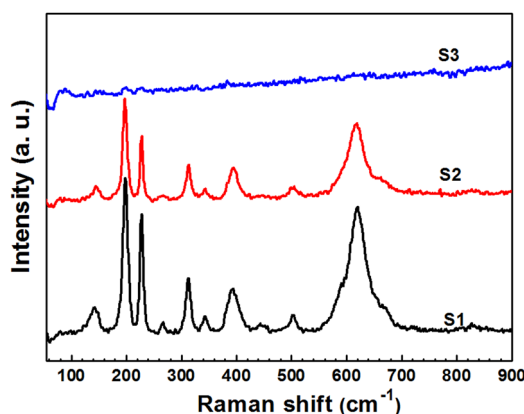


FIG. 4. Raman spectra of S1-S3 at RT.

based on XRD, that only VO<sub>2</sub> is present following hydrogen processing. The absence of a shift in the Raman peak positions, particularly the low-frequency V–V modes, is also consistent with the presence of coexisting M1 and R phases of VO<sub>2</sub> rather than a homogeneous, weakly hydrogenated material.

From Eq. (1), the required resistivity to achieve the ideal IMC for VO<sub>2</sub>/sapphire is  $\sim 2.41 \times 10^{-3} \Omega \cdot \text{cm}$ , given  $d \sim 120 \text{ nm}$ ,  $n_s \sim 3.0$  (at 1 THz). As shown in Fig. 2, this can be accomplished with S2 at RT where we anticipate negligible THz reflections at the sapphire-VO<sub>2</sub>/air interface. To verify this claim we show in Fig. 5 the THz transmission responses of S1-S3 at RT. In time domain (Fig. 5(a)), the waveforms consist primarily of two pulses: the main transmitted pulse and a second low intensity pulse (highlighted by the dash square) delayed by  $\sim 8.5 \text{ ps}$  from the first pulse. This secondary pulse is associated with one round-trip internal reflection (see Fig. 1(a)). Both S1 and S3 exhibited a pronounced second pulse. The second pulse observed in S1 is in-phase with the main transmitted one confirming the expected zero phase shift upon reflection. In contrast, the second pulse observed in S3 exhibits an 180° phase shift due to the metallic state of the VO<sub>2</sub> film. THz transmission measurements on S2 revealed negligible intensity for the second pulse, consistent with effective suppression of the reflection at the sapphire-VO<sub>2</sub>/air interface. This result demonstrates

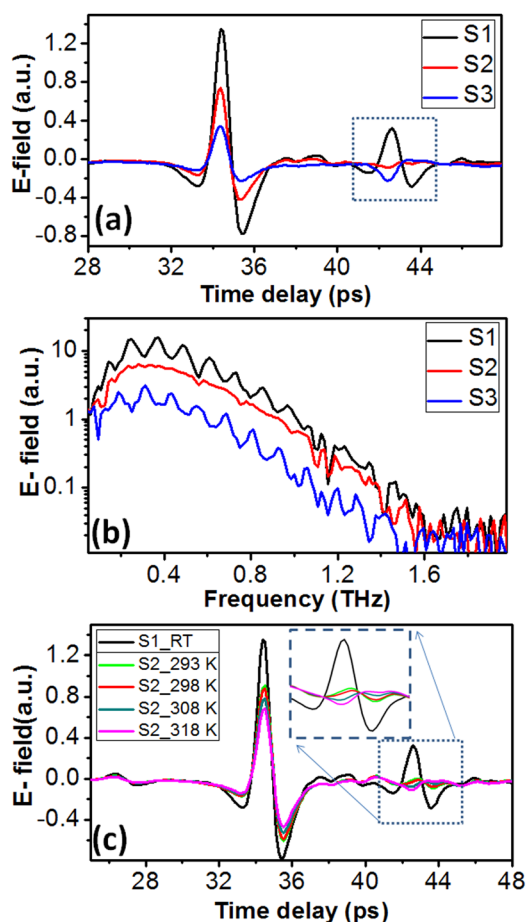


FIG. 5. THz transmission (a) time waveforms and (b) corresponding frequency spectra of S1-S3 at RT. (c) THz time waveforms of S2 at different temperatures. The inset is the zoom-in of the second pulses.

that IMC can be achieved at RT with hydrogenated VO<sub>2</sub>/sapphire films. We determined amplitude ratios between the second to the main pulse as 4.4%, 28.6%, and 38.5% for S2, S1, and S3, respectively. Figure 5(b) shows the corresponding frequency spectra of S1-S3 determined from Fig. 5(a). As expected, clear and well-pronounced frequency dependent resonances were observed for both S1 and S3, while S2 shows a smooth dependence confirming that the IMC is achieved at RT.

It is evident from the resistivity curve of S1 (see Fig. 2) that the IMC can be also obtained for this sample by tuning temperature within the MIT. However, the sharp resistivity variation and narrow hysteresis loop width observed for S1 during the MIT makes it significantly difficult to control. Slight temperature variations within the MIT will result in rapid deviations from the IMC. It is also interesting to note that the resistivity of S2 does not vary significantly in a temperature range of  $\sim 25 \text{ K}$  near RT. Therefore, the IMC for S2 can be achieved over a reasonable temperature range. To validate this point, we show in Fig. 5(c) results on THz transmission measurements for S2 at temperatures near the IMC. We determined amplitude ratios between the second pulse to the main one as 5.8%, 4.2%, 3.7%, and 7.4%, for temperatures of 293 K, 298 K, 308 K, and 318 K, respectively. The 180° phase shift between 298 K and 308 K can be observed, indicating that the minimum air-VO<sub>2</sub>/sapphire reflectivity should lie between these two temperatures. The results clearly demonstrate that hydrogen-doped VO<sub>2</sub> films can be used to achieve the desired IMC at RT for THz optics applications.

In summary, controlling the hydrogen spillover process permits changes of more than four orders of magnitude in the RT resistivity of VO<sub>2</sub> films. The hydrogen doping reduces the phase transition temperature of VO<sub>2</sub> and stabilizes its metallic phase at low temperature. Through precise control of doping, the resistivity can be tuned in order to achieve the desired IMC to suppress Fabry-Perot reflection at THz frequencies. We anticipate that the hydrogen doping approach will be an important step to realize high performance optical components for THz applications such as ultra-fast switches, filters, and beam splitters.

The authors acknowledge support for this work from NSF (No. ECCS 1128644).

<sup>1</sup>R. M. Wentzcovitch, W. W. Schulz, and P. B. Allen, *Phys. Rev. Lett.* **72**, 3389 (1994).

<sup>2</sup>A. S. Belozero, M. A. Korotin, V. I. Anisimov, and A. I. Poteryaev, *Phys. Rev. B* **85**, 045109 (2012).

<sup>3</sup>J. M. Tomczak, F. Aryasetiawan, and S. Biermann, *Phys. Rev. B* **78**, 115103 (2008).

<sup>4</sup>C. Wu, F. Feng, and Y. Xie, *Chem. Soc. Rev.* **42**, 5157 (2013).

<sup>5</sup>G. Stefanovich, A. Pergament, and D. Stefanovich, *J. Phys.: Condens. Matter* **12**, 8837 (2000).

<sup>6</sup>C. Chen, Y. Zhu, Y. Zhao, J. H. Lee, H. Wang, A. Bernussi, M. Holtz, and Z. Fan, *Appl. Phys. Lett.* **97**, 211905 (2010).

<sup>7</sup>Q. Shi, W. Huang, T. Lu, Y. Zhang, F. Yue, S. Qiao, and Y. Xiao, *Appl. Phys. Lett.* **104**, 071903 (2014).

<sup>8</sup>Y. Zhu, S. Vegesna, Y. Zhao, V. Kuryatkov, M. Holtz, Z. Fan, M. Saed, and A. A. Bernussi, *Opt. Lett.* **38**, 2382 (2013).

<sup>9</sup>Y. Zhu, Y. Zhao, M. Holtz, Z. Fan, and A. Bernussi, *J. Opt. Soc. Am. B* **29**, 2373 (2012).

<sup>10</sup>H.-W. Hübers, J. Schubert, A. Krabbe, M. Birk, G. Wagner, A. Semenov, G. Gol'tsman, B. Voronov, and E. Gershenzon, *Infrared Phys. Technol.* **42**, 41 (2001).

- <sup>11</sup>A. Thoman, A. Kern, H. Helm, and M. Walther, *Phys. Rev. B* **77**, 195405 (2008).
- <sup>12</sup>J. Kroll, J. Darmo, and K. Unterrainer, *Opt. Express* **15**, 6552 (2007).
- <sup>13</sup>C. Chen and Z. Fan, *Appl. Phys. Lett.* **95**, 262106 (2009).
- <sup>14</sup>S. S. N. Bharadwaja, C. Venkatasubramanian, N. Fieldhouse, S. Ashok, M. W. Horn, and T. N. Jackson, *Appl. Phys. Lett.* **94**, 222110 (2009).
- <sup>15</sup>Y. Zhao, C. Chen, X. Pan, Y. Zhu, M. Holtz, A. Bernussi, and Z. Fan, *J. Appl. Phys.* **114**, 113509 (2013).
- <sup>16</sup>K. M. Park, S. Yi, S. Moon, and S. Im, *Opt. Mater.* **17**, 311 (2001).
- <sup>17</sup>J. Nag and R. F. Haglund, Jr., *J. Phys.: Condens. Matter* **20**, 264016 (2008).
- <sup>18</sup>K. Shibuya, M. Kawasaki, and Y. Tokura, *Appl. Phys. Lett.* **96**, 022102 (2010).
- <sup>19</sup>C. Tang, P. Georgopoulos, M. E. Fine, J. B. Cohen, M. Nygren, G. S. Knapp, and A. Aldred, *Phys. Rev. B* **31**, 1000 (1985).
- <sup>20</sup>J. M. Booth and P. S. Casey, *Phys. Rev. Lett.* **103**, 086402 (2009).
- <sup>21</sup>X. Tan, T. Yao, R. Long, Z. Sun, Y. Feng, H. Cheng, X. Yuan, W. Zhang, Q. Liu, C. Wu, Y. Xie, and S. Wei, *Sci. Rep.* **2**, 466 (2012).
- <sup>22</sup>C. Wu, F. Feng, J. Feng, J. Dai, L. Peng, J. Zhao, J. Yang, C. Si, Z. Wu, and Y. Xie, *J. Am. Chem. Soc.* **133**, 13798 (2011).
- <sup>23</sup>P. Claus, *Appl. Catal. A* **291**, 222 (2005).
- <sup>24</sup>D. A. Panayotov and J. T. Yate, Jr., *J. Phys. Chem. C* **111**, 2959 (2007).
- <sup>25</sup>A. M. Chippindale, P. G. Dickens, and A. V. Powell, *J. Solid State Chem.* **93**, 526 (1991).
- <sup>26</sup>J. Wei, H. Ji, W. Guo, A. H. Nevidomskyy, and D. Natelson, *Nat. Nanotechnol.* **7**, 357 (2012).
- <sup>27</sup>C. Chen, Y. Zhao, X. Pan, V. Kuryatkov, A. Bernussi, M. Holtz, and Z. Fan, *J. Appl. Phys.* **110**, 023707 (2011).
- <sup>28</sup>B. S. Allimi, S. P. Alpay, C. K. Xie, B. O. Wells, J. I. Budnick, and D. M. Pease, *Appl. Phys. Lett.* **92**, 202105 (2008).
- <sup>29</sup>Joint Committee on Powder Diffraction Standards (JCPDS): 76-1043 and 74-1642.
- <sup>30</sup>K. Okimura, J. Sakai, and S. Ramanathan, *J. Appl. Phys.* **107**, 063503 (2010).
- <sup>31</sup>J. B. Goodenough, *J. Solid State Chem.* **3**, 490 (1971).
- <sup>32</sup>M. Nazari, C. Chen, A. A. Bernussi, Z. Y. Fan, and M. Holtz, *Appl. Phys. Lett.* **99**, 071902 (2011).